Computational Materials Science 174 (2020) 109477

Contents lists available at ScienceDirect

Computational Materials Science

journal homepage: www.elsevier.com/locate/commatsci

The effect of thermal history on the atomic structure and mechanical properties of amorphous alloys

Nikolai V. Priezjev[a,b,*]

[a] Department of Mechanical and Materials Engineering, Wright State University, Dayton, OH 45435, United States
[b] National Research University Higher School of Economics, Moscow 101000, Russia

ARTICLE INFO

Keyword:
Metallic glasses
Deformation
Thermal treatment
Yield stress
Molecular dynamics simulations

ABSTRACT

The influence of thermal processing on the potential energy, atomic structure, and mechanical properties of metallic glasses is examined using molecular dynamics simulations. We study the three-dimensional binary mixture, which was first relaxed near the glass transition temperature and zero pressure, and then rapidly cooled deep into the glass phase. It was found that glasses annealed at higher temperatures are relocated to higher energy states and their average glass structure remains more disordered, as reflected in the height of the first two peaks in the pair distribution function. The results of mechanical testing demonstrate that both the shear modulus and yielding peak increase significantly when the annealing temperature approaches T_g from above. Moreover, the shear modulus becomes a strong function of strain rate only for glasses relaxed at temperatures sufficiently higher than the glass transition temperature. Based on the spatial distribution of nonaffine displacements, we show that the deformation mode changes from brittle to ductile upon increasing annealing temperature. These results can be useful for the design and optimization of the fabrication processes of bulk glassy alloys with improved plasticity.

1. Introduction

Recent progress in the thermal treatment and deformation processing of amorphous alloys has resulted in a wider range of accessible energy states and optimized physical and mechanical properties [1]. It is well known that metallic glasses are much stronger than crystalline materials due to the absence of topological defects, or dislocations, but their deformation often proceeds via the formation of the so-called shear bands. Generally, aged samples become more brittle, while rejuvenated, or higher energy glasses, are more ductile. Common methods to rejuvenate metallic glasses and improve their plasticity include cold rolling, high pressure torsion, ion irradiation, and shot peening [2]. Interestingly, an application of elastostatic loading over extended time intervals can significantly rejuvenate metallic glasses due to plastic deformation of relatively soft domains [3–9]. A novel method to control rejuvenation consists of heating up metallic glasses slightly above the glass transition temperature, followed by rapid quenching back to the glass phase [10–13]. More recently, it was found that cryogenic thermal cycling might lead to higher energy states via local plastic events that are triggered because of the heterogeneity in the local thermal expansion [14–18]. In addition, it was demonstrated that the atomic structure and internal energy of amorphous materials can be tuned by cyclic deformation [19–32]. Finally, recent experimental studies showed that the ductile-to-brittle transition at room temperature is controlled by the so-called fictive temperature, which characterizes the average glass structure during a rapid quench below the glass transition temperature [33–35]. However, despite extensive efforts, the effect of thermo-mechanical processing on microstructure and mechanical properties of amorphous alloys remains not fully understood.

In this paper, we investigate the dependence of the potential energy, atomic structure and mechanical properties of binary glasses on the preparation protocol that consists of equilibration at an annealing temperature near the glass transition point and a subsequent quench to the test temperature. It will be shown that glasses prepared at lower annealing temperatures settle down at deeper potential energy minima and their short-range structure becomes more ordered. As a result, the shear modulus and stress overshoot depend strongly on the annealing temperature. We find that the rate dependence of the shear modulus becomes significant when the annealing temperature is greater than the glass transition temperature. The analysis of nonaffine displacements indicates that upon increasing annealing temperature, deformation changes from being localized within a shear band to more homogeneous.

* Address: Department of Mechanical and Materials Engineering, Wright State University, Dayton, OH 45435, United States.
E-mail address: nikolai.priezjev@wright.edu.

https://doi.org/10.1016/j.commatsci.2019.109477
Received 1 August 2019; Received in revised form 9 December 2019; Accepted 9 December 2019

This paper is organized as follows. The description of the molecular dynamics simulation model as well as the preparation and deformation protocols is provided in the next section. The dependence of the potential energy, radial distribution function, mechanical properties, and distribution of nonaffine displacements on the annealing temperature is presented in section 3. A brief summary is given in the last section.

2. Molecular dynamics simulation model

In this work, the structure and mechanical properties of an amorphous alloy are investigated by means of molecular dynamics simulations. We consider a well-studied binary (80:20) mixture originally introduced by Kob and Andersen (KA) about two decades ago [36]. The interaction parameters of the KA mixture are similar to the parametrization used by Weber and Stillinger to study the amorphous metal alloy $Ni_{80}P_{20}$ [37]. More specifically, the atoms of types $\alpha, \beta = A, B$ in the KA model interact via the Lennard-Jones (LJ) potential:

$$V_{\alpha\beta}(r) = 4\varepsilon_{\alpha\beta}\left[\left(\frac{\sigma_{\alpha\beta}}{r}\right)^{12} - \left(\frac{\sigma_{\alpha\beta}}{r}\right)^{6}\right], \quad (1)$$

with the following LJ parameters: $\varepsilon_{AA} = 1.0$, $\varepsilon_{AB} = 1.5$, $\varepsilon_{BB} = 0.5$, $\sigma_{AA} = 1.0$, $\sigma_{AB} = 0.8$, $\sigma_{BB} = 0.88$, and $m_A = m_B$ [36]. Note that this parametrization represents a system with strongly non-additive interaction between different types of atoms, which suppresses crystallization near the glass transition temperature [36]. The total number of atoms is $N = 60000$. To alleviate the computational load, the LJ potential was truncated at the cutoff radius $r_{c,\alpha\beta} = 2.5\sigma_{\alpha\beta}$. In what follows, all physical quantities are expressed in the LJ units of length, mass, energy, and time; namely, $\sigma = \sigma_{AA}$, $m = m_A$, $\varepsilon = \varepsilon_{AA}$, and $\tau = \sigma\sqrt{m/\varepsilon}$. The MD simulations were performed using the LAMMPS open-source, parallel code [38] with the integration time step $\Delta t_{MD} = 0.005\tau$.

The first step in the preparation procedure was to arrange all atoms at the sites of the fcc lattice and then equilibrate the binary mixture at the temperature $T_{LJ} = 1.0\varepsilon/k_B$ and zero pressure. Here, k_B and T_{LJ} indicate the Boltzmann constant and temperature, respectively. In all simulations, the system temperature was regulated via the Nosé-Hoover thermostat [39,38]. Periodic boundary conditions were imposed along all three dimensions. Next, the system was linearly cooled down to an annealing temperature T_a (in the vicinity of the glass transition temperature) during $10^4\tau$ at zero pressure. Once at T_a, the binary mixture was relaxed at constant temperature and pressure during the time interval $2 \times 10^5\tau$ (i.e., 4×10^7 MD steps). Following the relaxation period, the system was instantaneously quenched to the very low temperature $T_{LJ} = 0.01\varepsilon/k_B$ and then further relaxed during the additional time interval $10^4\tau$ at zero pressure.

After the thermal treatment, the mechanical properties were obtained by imposing shear strain deformation at constant volume and temperature $T_{LJ} = 0.01\varepsilon/k_B$. The shear modulus and the peak value of the stress overshoot were computed from the stress–strain curves, and the data were averaged over 15 independent samples. The deformation procedure was repeated for different values of the strain rate. This required substantial computational resources (about 1000 processors). In all simulations, the system temperature, potential energy, stress components, and atomic configurations were periodically saved for the post-processing analysis.

3. Results

It has been long realized that physical and mechanical properties of metallic glasses depend crucially on the annealing history [2]. An auxiliary concept to characterize the structural degrees of freedom is the so-called *fictive temperature* defined as the temperature at which the glass would be in equilibrium if suddenly brought to it from its current state [40,41]. In the limiting case of an infinitely fast quenching rate, used in the present study, the fictive temperature essentially coincides with the annealing temperature at which the system is equilibrated before the quench. Interestingly, it was demonstrated experimentally for different metallic glasses that an abrupt toughening transition between brittle and ductile regimes occurs as functions of the fictive temperature and strain rate [34]. It was argued that the mechanical transition originates from the competition between two time scales; the loading time, which is inversely proportional to the applied strain rate, and the plastic deformation time scale, determined by the density of plasticity carriers or shear transformation zones [34].

In the recent MD study, it was found that the glass transition temperature of the KA mixture of $N = 60000$ particles at zero pressure is $T_g \approx 0.35\varepsilon/k_B$ [13]. This value was obtained by linearly extrapolating the low and high temperature dependence of the potential energy during gradual cooling with the computationally slow rate of $10^{-5}\varepsilon/k_B\tau$. Note that higher cooling rates generally result in an increase of the glass transition temperature, which can be understood from the assumption that the relaxation time of the system follows a Vogel-Fulcher dependence on temperature [43]. For reference, the mode-coupling critical temperature of the KA model at the fixed density $\rho = 1.2\sigma^{-3}$ is $T_c = 0.435\varepsilon/k_B$, which was determined from the fit of the diffusion coefficients of either A or B types of particles to the power-law functions of temperature at constant volume [36].

In our study, the system was relaxed at zero pressure in the range of annealing temperatures, $0.31\varepsilon/k_B \leqslant T_a \leqslant 0.50\varepsilon/k_B$, near the glass transition temperature. The variation of the potential energy per particle during the relaxation time interval of $2 \times 10^5\tau$ and a subsequent quench to $T_{LJ} = 0.01\varepsilon/k_B$ is shown in Fig. 1 for selected values of the annealing temperature. It can be observed that the potential energy remains nearly constant at $T_a \gtrsim 0.38\varepsilon/k_B$, while it decreases gradually during aging at lower temperatures. To estimate the degree of structural relaxation during $2 \times 10^5\tau$, we computed the mean square displacement (MSD) of atoms at low annealing temperatures. For example, the averaged MSD is $r^2 \approx 1.64\sigma^2$ at $T_a = 0.32\varepsilon/k_B$, indicating that each atom undergoes a number of cage jumps during the relaxation time interval. This estimate is based on two atomic configurations separated by the time interval $2 \times 10^5\tau$.

After the system was equilibrated at a certain temperature near T_g, it was instantaneously quenched to the test temperature $T_{LJ} = 0.01\varepsilon/k_B$ and then relaxed during $10^4\tau$ at zero pressure. This procedure aims at freezing out the thermal vibrations but keeping intact the average glass structure. The inset in Fig. 1 shows the dependence of the potential

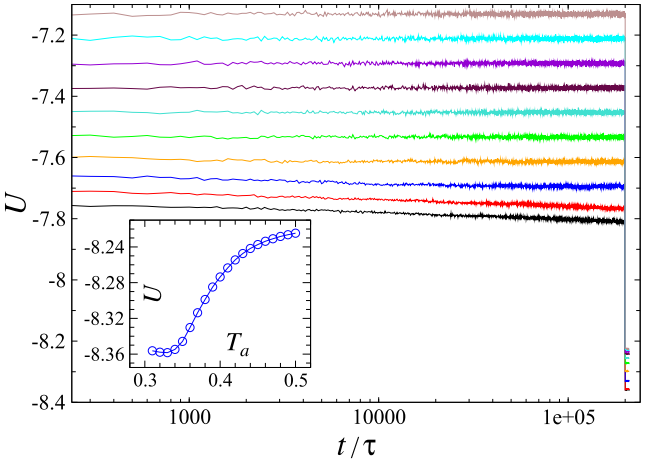

Fig. 1. The time dependence of the potential energy, U/ε, at various annealing temperatures, T_a, and after the quench to $T_{LJ} = 0.01\varepsilon/k_B$ at $P = 0$. The values of the annealing temperature are $T_a k_B/\varepsilon = 0.32$, 0.34, 0.36, 0.38, 0.40, 0.42, 0.44, 0.46, 0.48, and 0.50 (from bottom to top). The inset shows the potential energy at $T_{LJ} = 0.01\varepsilon/k_B$ after the time interval of $10^4\tau$. The data in the inset are averaged over 15 samples.

energy after $10^4\tau$ at $T_{LJ} = 0.01\,\varepsilon/k_B$ as a function of the annealing temperature. It can be seen that the potential energy, which is mostly determined by the glass structure, decreases towards a minimum when T_a approaches the glass transition temperature from above. These results confirm that the potential energy of inherent structures becomes lower when the temperature is reduced towards the glass transition temperature [44,20]. Test simulations at lower annealing temperatures, $0.28\,\varepsilon/k_B \leqslant T_a \leqslant 0.30\,\varepsilon/k_B$, have shown that U, measured at $T_{LJ} = 0.01\,\varepsilon/k_B$, continues to increase upon further reducing T_a (not shown). This trend can be explained by realizing that the effective cooling rate increases when the system temperature is reduced from $T_{LJ} = 1.0\,\varepsilon/k_B$ to lower values of T_a during the fixed time interval of $10^4\tau$. This way the system is annealed to a glass phase with higher energy states.

We next analyze the changes in the glass structure for systems prepared at different annealing temperatures. It was previously realized that the most sensitive measure of the atomic structure of the KA model glass is the shape of the pair correlation function of the smaller atoms of type B [43,42]. This conclusion stems from the fact that the interaction energy, ε_{BB} in Eq. (1), is the lowest among the three energies, and, therefore, the number of nearest-neighbor contacts between smaller, more mobile, atoms is reduced at lower temperatures [42]. In our study, the averaged pair distribution function is plotted in Fig. 2 for systems prepared at $T_a = 0.32\,\varepsilon/k_B$, $0.38\,\varepsilon/k_B$, and $0.50\,\varepsilon/k_B$. It can be readily observed that the height of the first peak is significantly reduced when the annealing temperature is varied from $0.50\,\varepsilon/k_B$ to $0.32\,\varepsilon/k_B$, while the opposite trend is seen for the second peak. We comment that the variation of the first peak height in Fig. 2 is much more pronounced than the change reported during the heat treatment process, where the glass structure was reset by heating above T_g and then the system was cooled back to the glass phase with different rates, resulting in slightly rejuvenated states [13].

The examples of stress–strain curves during shear deformation with the strain rate $\dot{\varepsilon}_{xz} = 10^{-5}\tau^{-1}$ are presented in Fig. 3 for selected values of T_a. The deformation was imposed at constant volume and temperature $T_{LJ} = 0.01\,\varepsilon/k_B$ up to 20% shear strain. As is evident, the stress response gradually changes from a monotonic increase and saturation at $T_a = 0.50\,\varepsilon/k_B$ to a pronounced overshoot followed by an abrupt stress drop at $T_a = 0.32\,\varepsilon/k_B$. Such behavior typically reflects either a uniform plastic flow of poorly annealed glasses or the formation of a shear band in well annealed samples (see discussion below).

The stress–strain curves were used to estimate the peak value of the

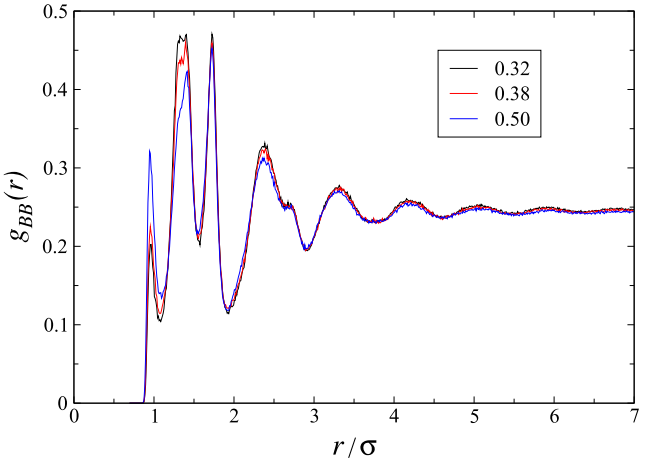

Fig. 2. The pair distribution function of smaller atoms of type B, $g_{BB}(r)$, for glasses prepared at different annealing temperatures. The values of T_a (in units of ε/k_B) are listed in the legend. The distribution function was computed after the samples were instantaneously quenched from T_a to $T_{LJ} = 0.01\,\varepsilon/k_B$ and then relaxed during the time interval $10^4\tau$ at $P = 0$. The data are averaged over 15 independent samples for each value of T_a.

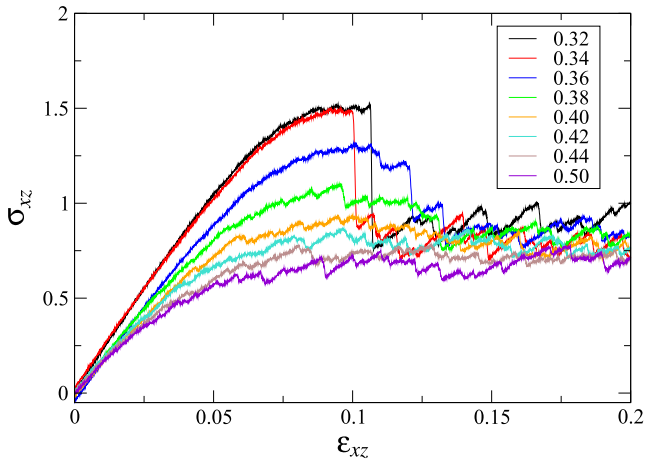

Fig. 3. The variation of shear stress, σ_{xz} (in units of $\varepsilon\sigma^{-3}$), as a function of strain, ε_{xz}, for the indicated values of the annealing temperature (see the legend). The samples were strained along the xz plane with the strain rate $\dot{\varepsilon}_{xz} = 10^{-5}\tau^{-1}$ at $T_{LJ} = 0.01\,\varepsilon/k_B$ and constant volume.

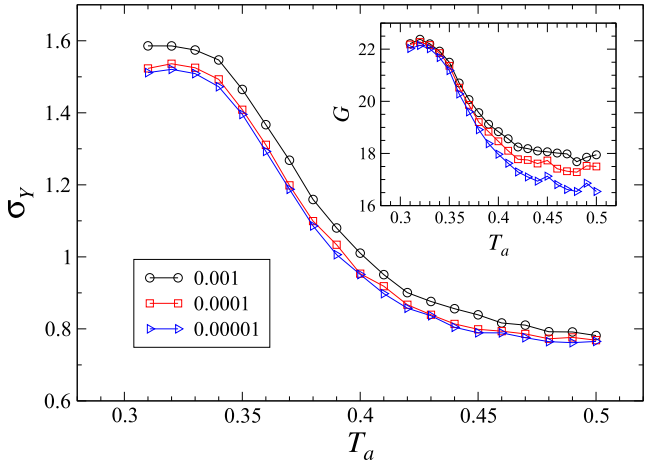

Fig. 4. The peak value of the stress overshoot σ_Y (in units of $\varepsilon\sigma^{-3}$) as a function of the annealing temperature for the indicated values of the strain rate, $\dot{\varepsilon}_{xz}$ (in units of τ^{-1}). The inset shows the shear modulus G (in units of $\varepsilon\sigma^{-3}$) versus T_a for the same strain rates. The data for σ_Y and G are averaged over 15 samples.

stress overshoot as a function of T_a. In turn, the shear modulus was computed from the slope of the best linear fit to the data at $\varepsilon_{xz} \leqslant 0.01$. Both σ_Y and G, averaged over 15 samples, are plotted in Fig. 4 for the indicated strain rates. It can be clearly seen that the mechanical properties depend strongly on the annealing temperature and the transition occurs when $T_a \approx T_g$. Furthermore, it was recently shown experimentally that a toughening transition as a function of strain rate becomes more pronounced when the fictive temperature is slightly higher than T_g [34]. In our MD setup, the yielding peak becomes higher with increasing strain rate, as expected; but the increase in σ_Y is rather insensitive to T_a (see Fig. 4). On the other hand, as shown in the inset to Fig. 4, the shear modulus is a strong function of strain rate only when $T_a > T_g$. In this sense, the results of MD simulations are consistent with the conclusions of the experimental study [34]. It should also be commented that it is difficult to access strain rates outside the range $10^{-5} \leqslant \dot{\varepsilon}_{xz}\tau \leqslant 10^{-3}$ reported in Fig. 4. Specifically, the averaging becomes computationally expensive at lower strain rates, while temperature oscillations are detected at higher strain rates.

The microscopic details of the deformation process can be captured via the analysis of the so-called nonaffine displacements of atoms [45]. It is well realized that the local displacement of an atom with respect to its neighbors can be computed via the transformation matrix $\mathbf{J}_i$, which

linearly transforms a group of atoms during the time interval Δt and at the same time minimizes the following quantity:

$$D^2(t, \Delta t) = \frac{1}{N_i} \sum_{j=1}^{N_i} \{\mathbf{r}_j(t + \Delta t) - \mathbf{r}_i(t + \Delta t) - \mathbf{J}_i[\mathbf{r}_j(t) - \mathbf{r}_i(t)]\}^2, \quad (2)$$

where the summation is carried over the neighbors within a sphere of radius 1.5σ with the center at the position vector $\mathbf{r}_i(t)$. It was demonstrated that the nonaffine measure is an excellent diagnostic of localized shear transformations in deformed amorphous materials [45]. Thus, recent studies on periodic deformation of disordered solids have shown that the amplitude of the nonaffine measure is approximately power-law distributed, while the majority of atoms rearrange reversibly during one or several subyield cycles [24,25]. Above the yielding point, the temporal evolution of spatial distributions of atoms with large nonaffine displacements illustrated the existence of a transient regime of periodic deformation, followed by the formation of shear bands in both poorly [29] and well [27] annealed binary glasses. More recently, the analysis of nonaffine displacements was used to study aging and rejuvenation during elastostatic loading [9] as well as the mechanical [28,29,31] and thermal [16] annealing processes in amorphous alloys.

The spatial distribution of nonaffine displacements during steady shear deformation with the strain rate $\dot{\varepsilon}_{xz} = 10^{-5}\tau^{-1}$ is plotted in Fig. 5 for $T_a = 0.32\varepsilon/k_B$, in Fig. 6 for $0.38\varepsilon/k_B$, and in Fig. 7 for $0.50\varepsilon/k_B$. The sequence of instantaneous snapshots are taken at shear strains $\varepsilon_{xz} = 0.05$, 0.10, 0.15, and 0.20, and the nonaffine measure, Eq. (2), was computed with respect to the atomic configuration at zero strain. It can be clearly seen in Fig. 5 that the shear deformation is accompanied by relatively small clusters of atoms with large nonaffine displacements at $\varepsilon_{xz} \leqslant 0.10$, and the shear band is formed and becomes fully developed along the *xy* plane at higher strains. This behavior is consistent with the stress response shown in Fig. 3 for $T_a = 0.32\varepsilon/k_B$, where the stress drop at $\varepsilon_{xz} \approx 0.11$ is associated with the formation of the shear band.

Next, as illustrated in Fig. 6, the deformation pattern remains similar for the sample prepared at the higher annealing temperature $T_a = 0.38\varepsilon/k_B$, except that the shear band appears to be thinner and it is oriented perpendicular to the plane of shear. Such orientation is allowed due to periodic boundary conditions, and it was observed in the previous MD simulations of binary glasses under steady and periodic shear deformation [46,27]. In sharp contrast, a more homogeneous plastic deformation is detected in glasses equilibrated at $T_a = 0.50\varepsilon/k_B$, as shown in Fig. 7. The inherent structure at this annealing temperature has the highest potential energy level (see the inset in Fig. 1) and, therefore, the largest number of shear transformation zones with low instability thresholds, resulting in homogeneous deformation. Altogether, these results demonstrate the importance of controlling the annealing temperature in order to optimize the mechanical properties of bulk metallic glasses and improve their plasticity.

4. Conclusions

In summary, molecular dynamics simulations were carried out to investigate the influence of the thermal treatment on the atomic structure and mechanical properties of disordered solids. A model glass was represented by the three-dimensional binary mixture with highly non-additive parametrization that prevents crystallization near the glass transition temperature. The binary mixture was first annealed near the glass transition at zero pressure, followed by an instantaneous quench and further relaxation at a very low temperature. It was demonstrated that the potential energy of the inherent structures is reduced and the height of the nearest-neighbor peak in the pair distribution function of smaller atoms decreases in glasses annealed at lower temperatures. The results of mechanical tests indicate that both the shear modulus and the yielding peak increase significantly when the annealing temperature is reduced towards the glass transition temperature. We also found that the strain rate dependence of the shear

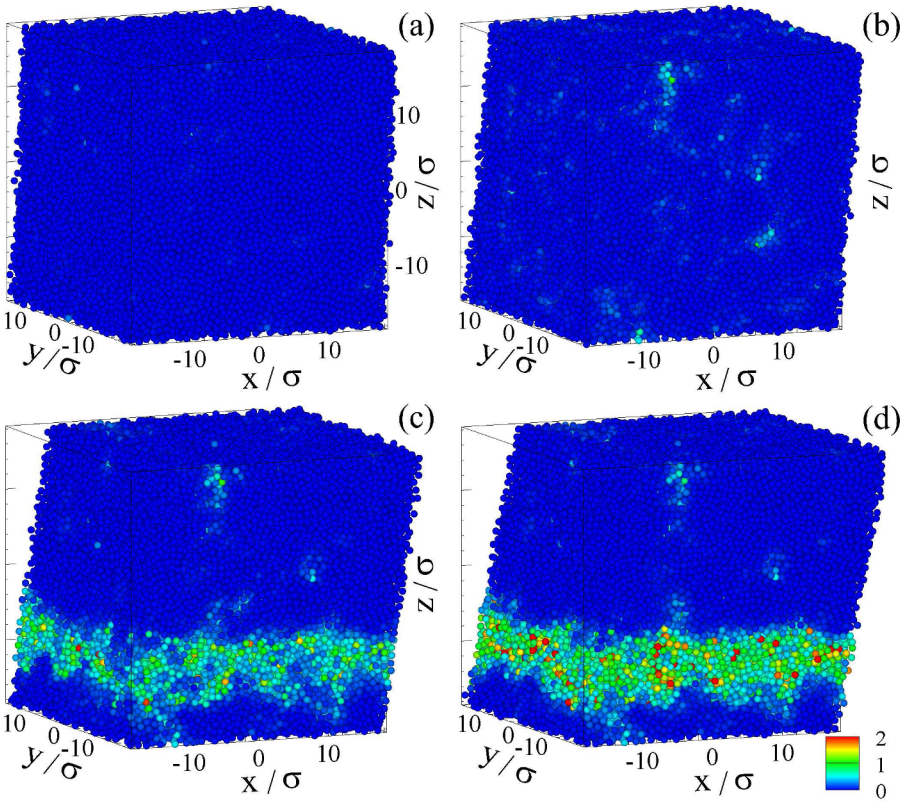

Fig. 5. The sequence of snapshots for the sample prepared at $T_a = 0.32\varepsilon/k_B$ and then quenched to $T_{LJ} = 0.01\varepsilon/k_B$. The shear strain ε_{xz} is (a) 0.05, (b) 0.10, (c) 0.15, and (d) 0.20. The rate of strain is $\dot{\varepsilon}_{xz} = 10^{-5}\tau^{-1}$. The color denotes the nonaffine measure D^2 with respect to zero strain (see the legend).

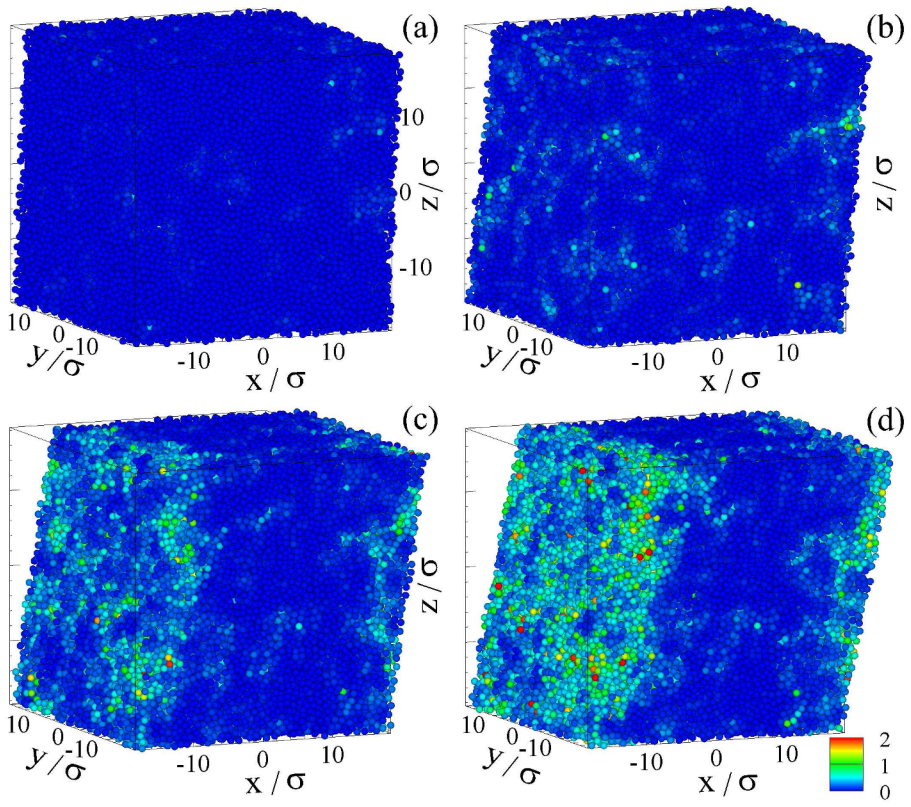

Fig. 6. The series of snapshots depicting atomic configurations in the strained glass prepared at the annealing temperature $T_a = 0.38\,\varepsilon/k_B$. The shear strain is (a) 0.05, (b) 0.10, (c) 0.15, and (d) 0.20. The nonaffine measure D^2 with respect to zero strain is marked according to the legend. The glass is strained at $T_{LJ} = 0.01\,\varepsilon/k_B$ and constant volume with the rate $\dot{\varepsilon}_{xz} = 10^{-5}\tau^{-1}$. The atoms are not drawn to scale.

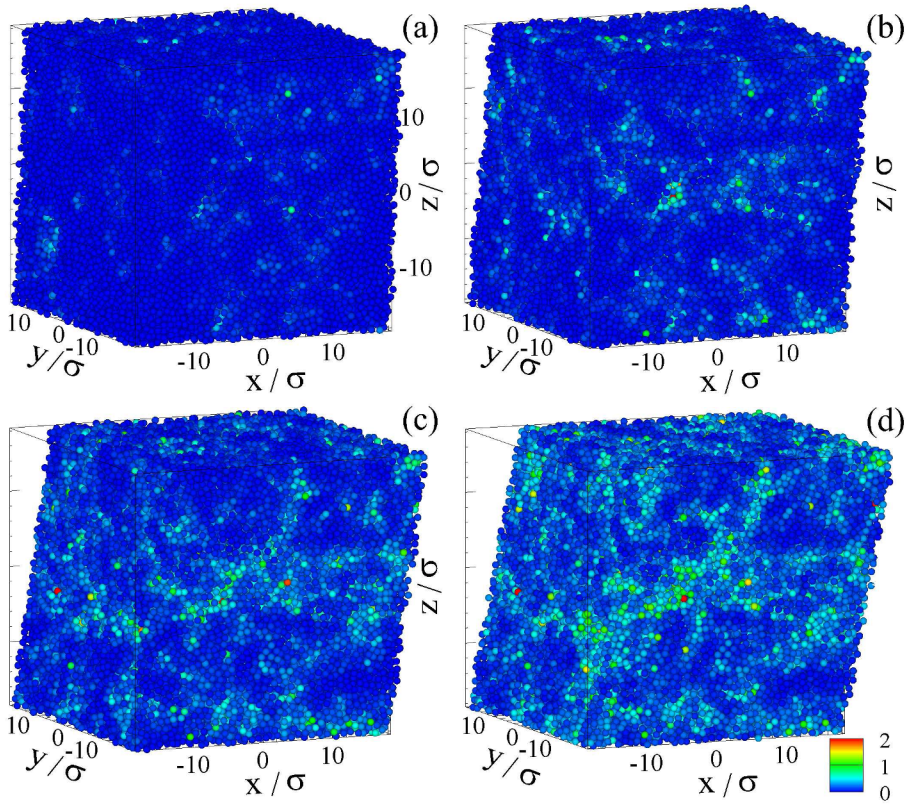

Fig. 7. The consecutive snapshots of the glass equilibrated at $T_a = 0.50\,\varepsilon/k_B$ and then quenched to $T_{LJ} = 0.01\,\varepsilon/k_B$. The strain is (a) 0.05, (b) 0.10, (c) 0.15, and (d) 0.20. The nonaffine displacements of atoms with respect to their neighbors at zero strain are indicated by the color according to the figure legend. The strain rate is $\dot{\varepsilon}_{xz} = 10^{-5}\tau^{-1}$.

modulus becomes pronounced in glasses relaxed at annealing temperatures greater than the glass transition temperature. The analysis of nonaffine displacements illustrated that the shear deformation changes from brittle to ductile upon increasing annealing temperature.

Declaration of Competing Interest

The authors declare that they have no known competing financial interests or personal relationships that could have appeared to influence the work reported in this paper.

Acknowledgments

Financial support from the National Science Foundation (CNS-1531923) is gratefully acknowledged. The article was prepared within the framework of the HSE University Basic Research Program and funded in part by the Russian Academic Excellence Project '5–100'. The molecular dynamics simulations were performed using the LAMMPS software developed at Sandia National Laboratories [38]. The numerical simulations were performed at Wright State University's Computing Facility and the Ohio Supercomputer Center.

References

[1] J.C. Qiao, Q. Wang, J.M. Pelletier, H. Kato, R. Casalini, D. Crespo, E. Pineda, Y. Yao, Y. Yang, Structural heterogeneities and mechanical behavior of amorphous alloys, Prog. Mater. Sci. 104 (2019) 250.
[2] Y. Sun, A. Concustell, A.L. Greer, Thermomechanical processing of metallic glasses: extending the range of the glassy state, Nat. Rev. Mater. 1 (2016) 16039.
[3] K.-W. Park, C.-M. Lee, M. Wakeda, Y. Shibutani, M.L. Falk, J.-C. Lee, Elastostatically induced structural disordering in amorphous alloys, Acta Mater. 56 (2008) 5440.
[4] Y. Tong, W. Dmowski, Y. Yokoyama, G. Wang, P.K. Liaw, T. Egami, Recovering compressive plasticity of bulk metallic glasses by high-temperature creep, Scr. Mater. 69 (2013) 570.
[5] A.L. Greer, Y.H. Sun, Stored energy in metallic glasses due to strains within the elastic limit, Philos. Mag. 96 (2016) 1643.
[6] M. Zhang, Y.M. Wang, F.X. Li, S.Q. Jiang, M.Z. Li, L. Liu, Mechanical relaxation-to-rejuvenation transition in a Zr-based bulk metallic glass, Sci. Rep. 7 (2017) 625.
[7] J. Pan, Y.X. Wang, Q. Guo, D. Zhang, A.L. Greer, Y. Li, Extreme rejuvenation and softening in a bulk metallic glass, Nat. Commun. 9 (2018) 560.
[8] M. Samavatian, R. Gholamipour, A.A. Amadeh, S. Mirdamadi, Role of tensile elastostatic loading on atomic structure and mechanical properties of $Zr_{55}Cu_{30}Ni_5Al_{10}$ bulk metallic glass, Mater. Sci. Eng. A 753 (2019) 218.
[9] N.V. Priezjev, Aging and rejuvenation during elastostatic loading of amorphous alloys: a molecular dynamics simulation study, Comput. Mater. Sci. 168 (2019) 125.
[10] M. Wakeda, J. Saida, J. Li, S. Ogata, Controlled rejuvenation of amorphous metals with thermal processing, Sci. Rep. 5 (2015) 10545.
[11] S. Kuchemann, P.M. Derlet, C. Liu, D. Rosenthal, G. Sparks, W.S. Larson, R. Maass, Energy storage in metallic glasses via flash annealing, Adv. Funct. Mater. 28 (2018) 1805385.
[12] M. Wang, H. Liu, J. Mo, Y. Zhang, Z. Chen, C. Yin, W. Yang, Thermal-pressure effects on energy state of metallic glass $Cu_{50}Zr_{50}$, Comput. Mater. Sci. 155 (2018) 493.
[13] N.V. Priezjev, Atomistic modeling of heat treatment processes for tuning the mechanical properties of disordered solids, J. Non-Cryst. Solids 518 (2019) 128.
[14] S.V. Ketov, Y.H. Sun, S. Nachum, Z. Lu, A. Checchi, A.R. Beraldin, H.Y. Bai, W.H. Wang, D.V. Louzguine-Luzgin, M.A. Carpenter, A.L. Greer, Rejuvenation of metallic glasses by non-affine thermal strain, Nature 524 (2015) 200.
[15] B. Shang, P. Guan, J.-L. Barrat, Role of thermal expansion heterogeneity in the cryogenic rejuvenation of metallic glasses, J. Phys.: Mater. 1 (2018) 015001 .
[16] N.V. Priezjev, The effect of cryogenic thermal cycling on aging, rejuvenation, and mechanical properties of metallic glasses, J. Non-Cryst. Solids 503 (2019) 131.
[17] Q.-L. Liu, N.V. Priezjev, The influence of complex thermal treatment on mechanical properties of amorphous materials, Comput. Mater. Sci. 161 (2019) 93.
[18] W. Guo, J. Saida, M. Zhao, S. Lu, S. Wu, Rejuvenation of Zr-based bulk metallic glass matrix composite upon deep cryogenic cycling, Mater. Lett. 247 (2019) 135.
[19] N.V. Priezjev, Heterogeneous relaxation dynamics in amorphous materials under cyclic loading, Phys. Rev. E 87 (2013) 052302 .
[20] D. Fiocco, G. Foffi, S. Sastry, Oscillatory athermal quasistatic deformation of a model glass, Phys. Rev. E 88 (2013) 020301(R).
[21] I. Regev, T. Lookman, C. Reichhardt, Onset of irreversibility and chaos in amorphous solids under periodic shear, Phys. Rev. E 88 (2013) 062401 .
[22] N.V. Priezjev, Dynamical heterogeneity in periodically deformed polymer glasses, Phys. Rev. E 89 (2014) 012601 .
[23] I. Regev, J. Weber, C. Reichhardt, K.A. Dahmen, T. Lookman, Reversibility and criticality in amorphous solids, Nat. Commun. 6 (2015) 8805.
[24] N.V. Priezjev, Reversible plastic events during oscillatory deformation of amorphous solids, Phys. Rev. E 93 (2016) 013001 .
[25] N.V. Priezjev, Nonaffine rearrangements of atoms in deformed and quiescent binary glasses, Phys. Rev. E 94 (2016) 023004 .
[26] P. Leishangthem, A.D.S. Parmar, S. Sastry, The yielding transition in amorphous solids under oscillatory shear deformation, Nat. Commun. 8 (2017) 14653.
[27] N.V. Priezjev, Collective nonaffine displacements in amorphous materials during large-amplitude oscillatory shear, Phys. Rev. E 95 (2017) 023002 .
[28] N.V. Priezjev, Molecular dynamics simulations of the mechanical annealing process in metallic glasses: Effects of strain amplitude and temperature, J. Non-Cryst. Solids 479 (2018) 42.
[29] N.V. Priezjev, The yielding transition in periodically sheared binary glasses at finite temperature, Comput. Mater. Sci. 150 (2018) 162.
[30] Y.C. Lo, H.S. Chou, Y.T. Cheng, J.C. Huang, J.R. Morris, P.K. Liaw, Structural relaxation and self-repair behavior in nano-scaled Zr-Cu metallic glass under cyclic loading: molecular dynamics simulations, Intermetallics 18 (2010) 954.
[31] N.V. Priezjev, Slow relaxation dynamics in binary glasses during stress-controlled, tension-compression cyclic loading, Comput. Mater. Sci. 153 (2018) 235.
[32] N.V. Priezjev, Accelerated relaxation in disordered solids under cyclic loading with alternating shear orientation, J. Non-Cryst. Solids 525 (2019) 119683 .
[33] G. Kumar, P. Neibecker, Y.H. Liu, J. Schroers, Critical fictive temperature for plasticity in metallic glasses, Nat. Commun. 4 (2013) 1536.
[34] J. Ketkaew, W. Chen, H. Wang, A. Datye, M. Fan, G. Pereira, U.D. Schwarz, Z. Liu, R. Yamada, W. Dmowski, M.D. Shattuck, C.S. O'Hern, T. Egami, E. Bouchbinder, J. Schroers, Mechanical glass transition revealed by the fracture toughness of metallic glasses, Nat. Commun. 9 (2018) 3271.
[35] Z. Chen, A. Datye, P.A. Brooks, M. Sprole, J. Ketkaew, S. Sohn, J. Schroers, U.D. Schwarz, Dependence of modulus and hardness on the annealing conditions of $Pt_{57.5}Cu_{14.7}Ni_{5.3}P_{22.5}$ bulk metallic glass, MRS, Advances 4 (2019) 73.
[36] W. Kob, H.C. Andersen, Testing mode-coupling theory for a supercooled binary Lennard-Jones mixture: the van Hove correlation function, Phys. Rev. E 51 (1995) 4626.
[37] T.A. Weber, F.H. Stillinger, Local order and structural transitions in amorphous metal-metalloid alloys, Phys. Rev. B 31 (1985) 1954.
[38] S.J. Plimpton, Fast parallel algorithms for short-range molecular dynamics, J. Comput. Phys. 117 (1995) 1.
[39] M.P. Allen, D.J. Tildesley, Computer Simulation of Liquids, Clarendon, Oxford, 1987.
[40] A.Q. Tool, Relation between inelastic deformability and thermal expansion of glass in its annealing range, J. Am. Ceram. Soc. 29 (1946) 240.
[41] S. Richter, F. Zimmermann, A. Tunnermann, S. Nolte, Laser welding of glasses at high repetition rates – fundamentals and prospects, Opt. Laser Technol. 83 (2016) 59.
[42] M. Utz, P.G. Debenedetti, F.H. Stillinger, Atomistic simulation of aging and rejuvenation in glasses, Phys. Rev. Lett. 84 (2000) 1471.
[43] K. Vollmayr, W. Kob, K. Binder, How do the properties of a glass depend on the cooling rate? A computer simulation study of a Lennard-Jones system, J. Chem. Phys. 105 (1996) 4714.
[44] F.H. Stillinger, T.A. Weber, Packing structures and transitions in liquids and solids, Science 225 (1984) 983.
[45] M.L. Falk, J.S. Langer, Dynamics of viscoplastic deformation in amorphous solids, Phys. Rev. E 57 (1998) 7192.
[46] G.P. Shrivastav, P. Chaudhuri, J. Horbach, Yielding of glass under shear: a directed percolation transition precedes shear-band formation, Phys. Rev. E 94 (2016) 042605 .